



# Synthesis of Mo<sub>2</sub>C and W<sub>2</sub>C Nanoparticle Electrocatalysts for the Efficient Hydrogen Evolution Reaction in Alkali and Acid Electrolytes

Sajjad Hussain<sup>1,2</sup>, Dhanasekaran Vikraman<sup>3</sup>, Asad Feroze<sup>1,4</sup>, Wooseok Song<sup>5</sup>, Ki-Seok An<sup>5</sup>, Hyun-Seok Kim<sup>3</sup>, Seung-Hyun Chun<sup>1,4</sup> and Jongwan Jung<sup>1,2\*</sup>

<sup>1</sup> Graphene Research Institute, Sejong University, Seoul, South Korea, <sup>2</sup> Department of Nano and Advanced Materials Engineering, Sejong University, Seoul, South Korea, <sup>3</sup> Division of Electronics and Electrical Engineering, Dongguk University-Seoul, Seoul, South Korea, <sup>4</sup> Department of Physics, Sejong University, Seoul, South Korea, <sup>5</sup> Thin Film Materials Research Center, Korea Research Institute of Chemical Technology, Daejeon, South Korea

## OPEN ACCESS

### Edited by:

Yao Zheng,  
University of Adelaide, Australia

### Reviewed by:

Bao Yu Xia,  
Huazhong University of Science and  
Technology, China  
Shichun Mu,  
Wuhan University of  
Technology, China

### \*Correspondence:

Jongwan Jung  
jwjung@sejong.ac.kr

### Specialty section:

This article was submitted to  
Electrochemistry,  
a section of the journal  
Frontiers in Chemistry

Received: 14 August 2019

Accepted: 10 October 2019

Published: 25 October 2019

### Citation:

Hussain S, Vikraman D, Feroze A,  
Song W, An K-S, Kim H-S, Chun S-H  
and Jung J (2019) Synthesis of Mo<sub>2</sub>C  
and W<sub>2</sub>C Nanoparticle  
Electrocatalysts for the Efficient  
Hydrogen Evolution Reaction in Alkali  
and Acid Electrolytes.  
Front. Chem. 7:716.  
doi: 10.3389/fchem.2019.00716

The synthesis of low cost, high efficacy, and durable hydrogen evolution electrocatalysts from the non-noble metal group is a major challenge. Herein, we establish a simple and inexpensive chemical reduction method for producing molybdenum carbide (Mo<sub>2</sub>C) and tungsten carbide (W<sub>2</sub>C) nanoparticles that are efficient electrocatalysts in alkali and acid electrolytes for hydrogen evolution reactions (HER). Mo<sub>2</sub>C exhibits outstanding electrocatalytic behavior with an overpotential of −134 mV in acid medium and of −116 mV in alkaline medium, while W<sub>2</sub>C nanoparticles require an overpotential of −173 mV in acidic medium and −130 mV in alkaline medium to attain a current density of 10 mA cm<sup>−2</sup>. The observed results prove the capability of high- and low-pH active electrocatalysts of Mo<sub>2</sub>C and W<sub>2</sub>C nanoparticles to be efficient systems for hydrogen production through HER water electrolysis.

**Keywords:** Mo<sub>2</sub>C, W<sub>2</sub>C, nanoparticle, HER, electrocatalyst

## INTRODUCTION

A direct and effective route to clean and renewable hydrogen (H<sub>2</sub>) production by water splitting requires a robust catalyst to ensure sustainable efficiency (Vikraman et al., 2017). Platinum (Pt)-based systems are recognized as highly energetic HER catalysts that boast various pH tolerances and almost zero overpotential, but their high cost, originating from the scarcity of platinum, severely hinders their extensive use (Jacobsson et al., 2013; Peng et al., 2014). To reduce the use of Pt, intensive research has been conducted to prepare low-cost, highly active, and electrochemically stable HER electrocatalysts comprised of abundant elements as an alternative (Vikraman et al., 2018; Hussain et al., 2019a). Numerous types of non-scarce transition metal compounds, such as layered transition metal dichalcogenides (LTMDs) (Laursen et al., 2012; Seok et al., 2017; Hussain et al., 2018), phosphides (Lv and Wang, 2017; Pei et al., 2018), transition metal carbides (TMC) (Huang et al., 2016; Shi et al., 2017), and their composites (Ren et al., 2018; Vikraman et al., 2019b) have been shown to produce excellent HER activities because of their unique electronic structures. Various molybdenum selenide (MoSe<sub>2</sub>)-based materials, in particular, have been reported as being

suited for replacing Pt in HER electrocatalysts (Ren et al., 2018; Hussain et al., 2019a; Vikraman et al., 2019a). In addition, attaching Mo<sub>2</sub>C and W<sub>2</sub>C to a carbon matrix has been shown to produce high-rate charge transfer properties during HER and to alleviate surface aggregation (Pan et al., 2014; Youn et al., 2014; Wu et al., 2016). Previous reports suggested that the HER electrocatalytic performance of Mo<sub>2</sub>C- and W<sub>2</sub>C-based catalysts mainly results from the morphology (Ang et al., 2016; Ishii et al., 2016; Peng et al., 2017), crystalline phases (Wan et al., 2014; Lin et al., 2017), and composition (Yu et al., 2018; Zhang et al., 2018) of the catalysts and the synthetic protocol. However, the critical challenge is to design and develop carbide-based catalysts with comparable catalytic performance to Pt for practical applications. Until now, carbide-based materials have shown inferior catalytic properties due to their poor activities (Wu et al., 2016; Yu et al., 2018; Zhang et al., 2018). An earlier study reported the HER behavior of commercially available Mo<sub>2</sub>C meshes in both basic and acidic solutions, showing a comparatively high overpotential of  $-190\sim-230$  mV at a cathodic current of  $10\text{ mA cm}^{-2}$  (Vrubel and Hu, 2012). Performance has since been upgraded by tuning its nanocrystal size (Ma R. et al., 2015; Chen et al., 2016). Hence, Mo<sub>2</sub>C and W<sub>2</sub>C nanoparticles with high catalytic activity and robustness remain open for future research.

Various methods have been employed to prepare TMC-based catalysts (Wu et al., 2016; Zhu et al., 2016; An and Xu, 2019). Gong et al. obtained WC<sub>x</sub>/MoC<sub>x</sub>-based electrocatalysts by carbonizing W/WO<sub>3</sub> or Mo/MoO<sub>3</sub> under the flow of carbon precursors (C<sub>2</sub>H<sub>6</sub>, CH<sub>4</sub>, or CO, and H<sub>2</sub>), but very low surface areas were obtained (Gong et al., 2016). Tantalum carbide nanocrystals have been prepared via a refined Cl<sub>2</sub>-assisted “micro-cutting-fragmentation” approach and produced an overpotential of  $\sim-146$  mV@ $10\text{ mA cm}^{-2}$  for HER (Kou et al., 2017). Different methodologies have been used to prepare Mo<sub>2</sub>C and its hybrids for HER applications (Pu et al., 2016; Kou et al., 2018; Liang et al., 2019). Tungsten carbides can exist in different phases, such as WC, metastable W<sub>2</sub>C, and WC<sub>1-x</sub>, but during the last decade, most researchers have exclusively focused on the WC phase instead of the W<sub>2</sub>C phase (Neylon et al., 1999; Ishii et al., 2016). W/WC synthesized by Kou et al. (2019) showed an overpotential of  $159\text{ mV @ }10\text{ mA cm}^{-2}$ . As per experimental and theoretical calculations, the W<sub>2</sub>C phase exhibits more HER active catalytic properties than does WC, with a low negative Gibbs free energy ( $\Delta G_H$ ) for hydrogen adsorption and high Fermi level electronic density of states (DOS) (Colton et al., 1975; Gong et al., 2016).  $\beta$ -phase Mo<sub>2</sub>C and the W<sub>2</sub>C phase, in particular, have been validated as effective HER electrocatalysts despite their bulky natures, and their activity could be further increased by engineering with appropriate nanosize structures (Huang et al., 2016).

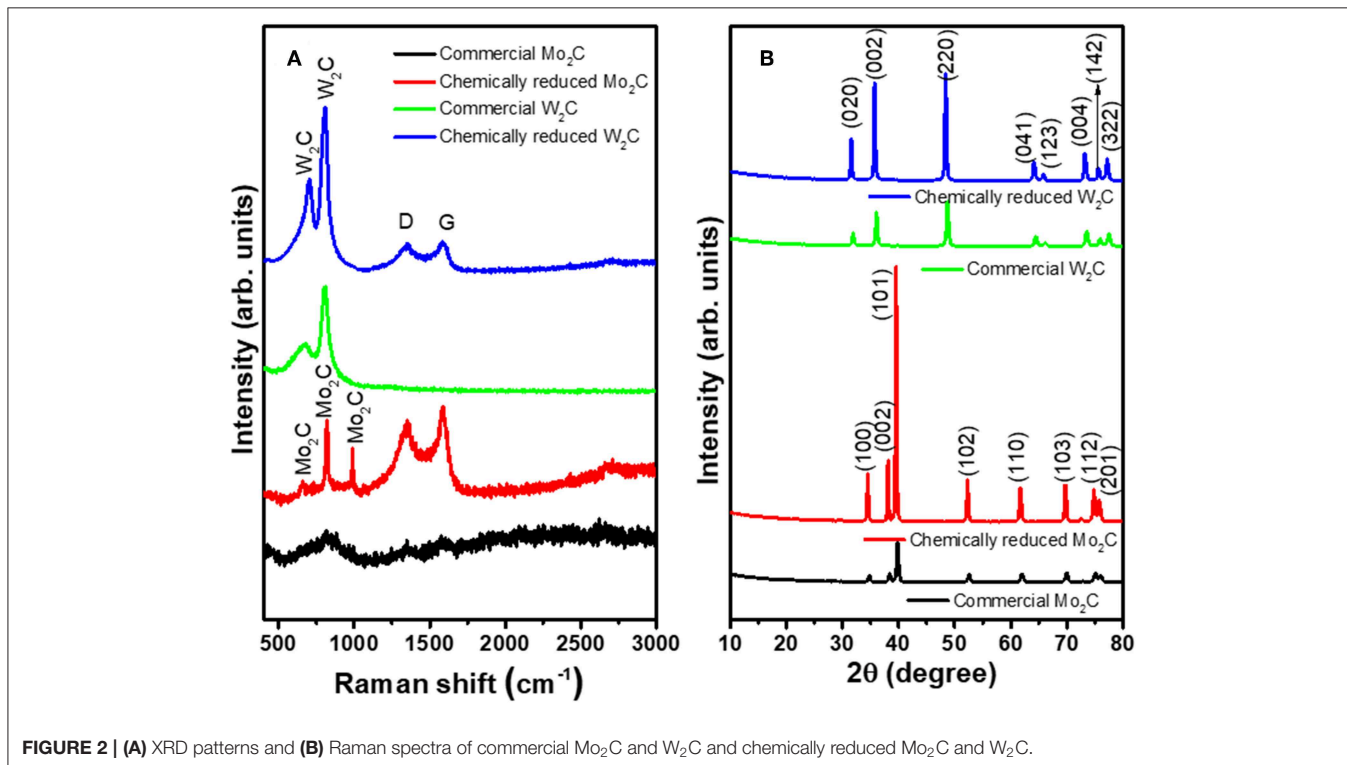
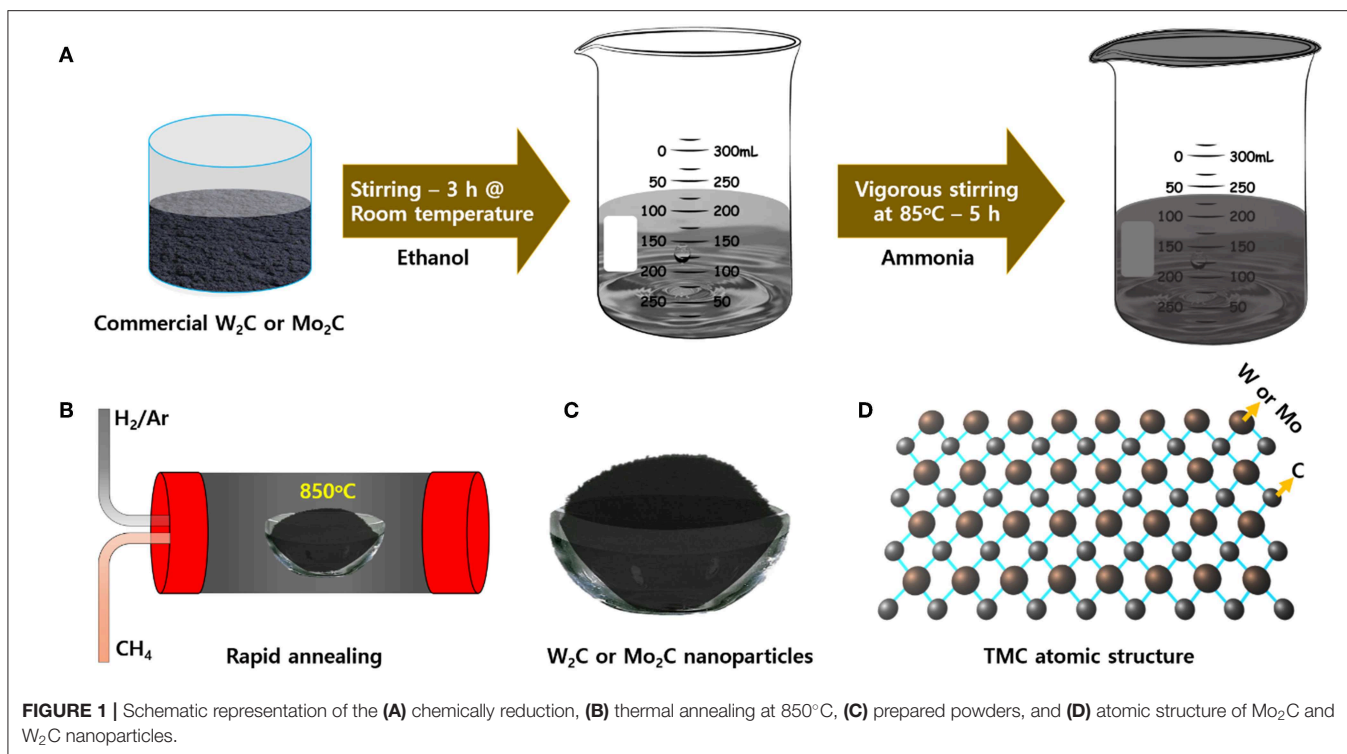
Herein, we have successfully synthesized Mo<sub>2</sub>C and W<sub>2</sub>C nanoparticles for HER application via a simple and economical chemical reduction method. The electrochemical results indicate that Mo<sub>2</sub>C nanoparticles exhibit superior HER electrocatalytic behavior over W<sub>2</sub>C in both alkaline and acid solutions, with small Tafel slopes and distinct solidity. We believe that our present investigation provides effective strategies for designing and preparing the new nanostructured TMC-based HER catalysts.

## RESULTS AND DISCUSSION

The chemically reduced synthesis scheme and the atomic structures of the Mo<sub>2</sub>C and W<sub>2</sub>C nanoparticles are pictorially represented in **Figure 1**. Raman characterization was performed for structural confirmation of commercial and chemically reduced Mo<sub>2</sub>C and W<sub>2</sub>C nanoparticles. **Figure 2A** shows the Raman spectra of commercial Mo<sub>2</sub>C and W<sub>2</sub>C and chemically reduced Mo<sub>2</sub>C and W<sub>2</sub>C. The commercial Mo<sub>2</sub>C revealed unclear peaks, whereas the chemically reduced Mo<sub>2</sub>C produced distinctive peaks at  $661$ ,  $818$ , and  $990\text{ cm}^{-1}$ , credited to  $\beta$ -Mo<sub>2</sub>C (Hussain et al., 2019b). In addition, the G band was positioned at  $1,582\text{ cm}^{-1}$  and the D band was positioned at  $1,349\text{ cm}^{-1}$ , which corresponds to the sp<sup>2</sup>-bonded carbon atoms and disarranged graphite carbon, respectively (Ma F. et al., 2015). The intensity ratio of the D-band to the G-band (i.e., I<sub>D</sub>/I<sub>G</sub>) is 0.85 for Mo<sub>2</sub>C, comparable to long-time carbonized graphene layers with high conductivity, which may facilitate charge transfer during HER (Li et al., 2016; Lv et al., 2017; Wang et al., 2017). For commercial and chemically reduced W<sub>2</sub>C, the strong peaks observed at  $693$  and  $807\text{ cm}^{-1}$  originate from the stretching vibration of W-C (Yan et al., 2017). The D and G bands were exhibited at  $1,351$  and  $1,583\text{ cm}^{-1}$  for the chemically reduced W<sub>2</sub>C (Yan et al., 2017; Zhang et al., 2018). The observed results are in good agreement with previous reports (Yan et al., 2017; Hussain et al., 2019a).

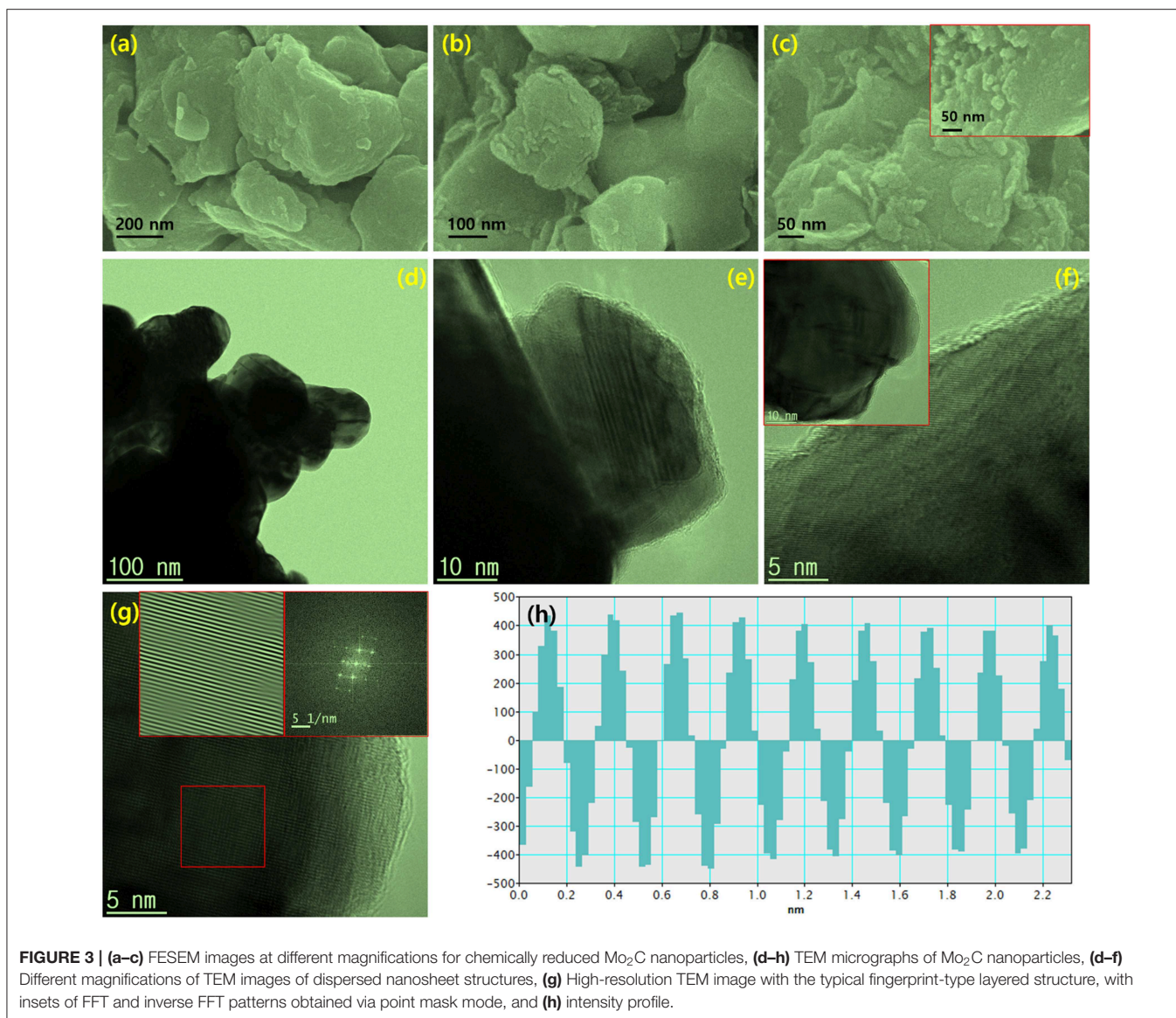
X-ray diffraction (XRD) was investigated to reveal the material structure of the commercial and chemical Mo<sub>2</sub>C and W<sub>2</sub>C nanoparticles (**Figure 2B**). For Mo<sub>2</sub>C, the XRD patterns revealed reflections at  $34.5$ ,  $38.1$ ,  $39.5$ ,  $52.3$ ,  $61.7$ ,  $69.6$ ,  $74.7$ , and  $75.7^\circ$ , which were indexed to the (100), (002), (101), (102), (110), (103), (112), and (201) planes of  $\beta$ -Mo<sub>2</sub>C (JCPDS: 35-0787), which is the most active phase of Mo<sub>2</sub>C for HER. In the case of W<sub>2</sub>C, the XRD patterns produced peaks at  $31.5$ ,  $35.1$ ,  $48.8$ ,  $64.1$ ,  $65.8$ ,  $73.2$ ,  $75.6$ , and  $77.1^\circ$  due to the (020), (002), (220), (041), (123), (004), (142), and (322) lattice planes, respectively (JCPDS: 89-2371). Compared with commercial samples, the chemically reduced samples showed higher-intensity peaks, which can be attributed to the enriched crystallinity in the nanoparticles compared to in bulk (Hussain et al., 2019a). No discernible peaks in either the Mo<sub>2</sub>C or W<sub>2</sub>C samples could be assigned to Mo/W, carbide, or other Mo/W non-stoichiometric phases and impurities, indicating the capability of the synthetic method to prepare effective nanostructures from bulk.

Morphology and microstructure modifications were inspected using field emission scanning electron microscopy (FESEM) and transmission electron microscopy (TEM). **Figures 3a–c** show FESEM images for reduced Mo<sub>2</sub>C nanoparticles. The observed images clearly indicated that larger sized grains were constructed through the accumulation of spherically shaped nanoparticles. The composition of reduced Mo<sub>2</sub>C nanoparticles was examined by energy dispersive spectroscopy (EDS), as shown in **Figure S1**. The observed composition of the chemically reduced sample is in good agreement with the claim of Mo<sub>2</sub>C formation, and EDS mapping images for the nanoparticles are provided in **Figure S2**. TEM images at different magnifications of Mo<sub>2</sub>C nanoparticles are provided in **Figures 3d–g**. The large grains are clearly seen in the lower-magnification TEM image (**Figure 3d**), and the typical



2D layered structures are shown in the higher-magnification images. A high-resolution TEM image showing a fingerprint-like structure is shown in **Figure 3g**, and its fast Fourier

transform (FFT) and inverse FFTs are inserted. The intensity profile extracted proved the existence of (101) lattice plane spacing (0.228 nm) between the fringes, as shown in **Figure 3h**.

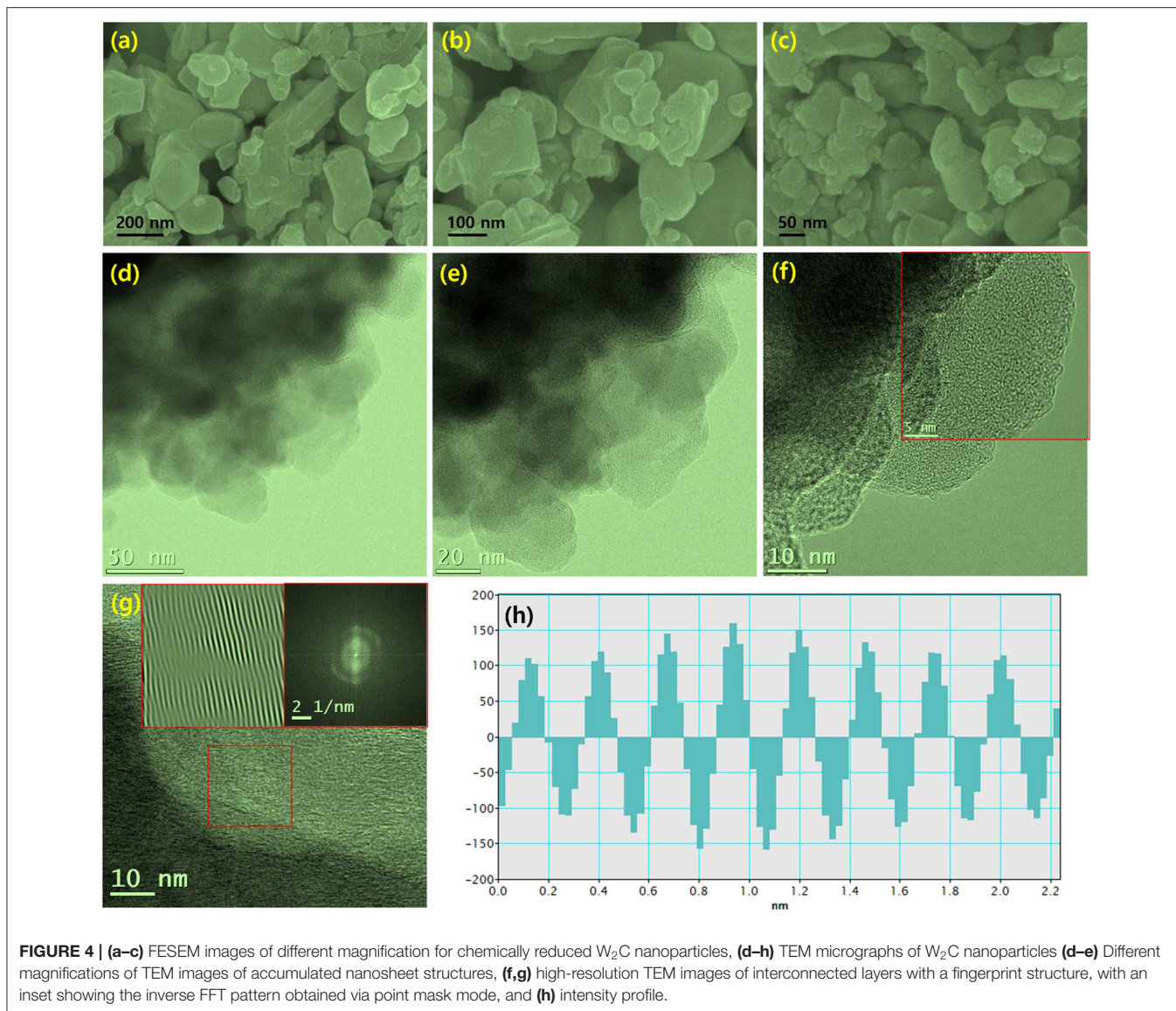


Hence, the microscopic images clearly proved the formation of Mo<sub>2</sub>C nanoparticles.

**Figure 4** shows FESEM and TEM images of chemically reduced W<sub>2</sub>C nanoparticles. The nanoparticles consist of inhomogeneous grains (**Figures 4a–c**). The EDS spectrum confirmed the existence of W<sub>2</sub>C nanoparticles (**Figure S3**), and their mapping images further supported the claim of W<sub>2</sub>C nanoparticle formation (**Figure S4**). The TEM images provided valuable insights regarding the W<sub>2</sub>C nanoparticles (**Figures 4d–g**). The irregularly sized nanograins were clearly seen in the low- and higher-magnification TEM images (**Figures 4f,g**). The FFT image showed the (002) W<sub>2</sub>C plane (0.26 nm spacing) (**Figure 4h**). The observed results are well-correlated with the XRD results.

An X-ray photoelectron spectroscopy (XPS) study was conducted to validate the composition of reduced Mo<sub>2</sub>C and

W<sub>2</sub>C. The XPS survey spectra revealed the occurrence of Mo<sub>2</sub>C (C and Mo)- and W<sub>2</sub>C (C and W)-based elements, as shown in **Figures S5A,B**. **Figure 5A** shows the de-convoluted high-resolution region for Mo 3d, with the Mo 3d<sub>5/2</sub> and Mo 3d<sub>3/2</sub> peaks at 228.6 and 231.9 eV, which reveals the carbidic Mo phase. The peaks at 233.3 and 235.9 eV are from molybdenum oxide (Mo<sup>6+</sup>), indicating surface oxidation in an air environment (Cui et al., 2014; Tang et al., 2015; Huang et al., 2016; Fan et al., 2018; Hussain et al., 2019a). The C 1s spectrum (**Figure 5B**) at a 284.8 eV binding energy is characteristic of the sp<sup>2</sup> carbon relation in Mo<sub>2</sub>C, whereas a satellite peak emerges at 288.8 eV due to C–O bonding (Wu et al., 2016). **Figure 5C** shows the high-resolution W 4f XPS spectrum from chemically reduced W<sub>2</sub>C. The deconvoluted peaks revealed at 31.64 and 33.81 eV were credited to 4f<sub>7/2</sub> and 4f<sub>5/2</sub>, respectively, for the W 4f atom. The high-resolution C 1s spectrum (**Figure 5D**) of W<sub>2</sub>C exposed the sp<sup>2</sup> graphitic carbon peak at 283.02 eV and C=O



peak at 285.1 eV (Berglund et al., 2014; Ko et al., 2017). The observed results confirmed the formation of Mo<sub>2</sub>C and W<sub>2</sub>C, which is in good agreement with the earlier literature (Ma F. et al., 2015; Yan et al., 2017). The surface area modifications were measured by the nitrogen (N<sub>2</sub>) adsorption/desorption isotherms for chemically reduced Mo<sub>2</sub>C and W<sub>2</sub>C nanoparticles via the Brunauer Emmett Teller (BET) method (Figures S6A,B). Surface area of 0.91 and 1.75 m<sup>2</sup>·g<sup>-1</sup> were observed for the chemically reduced Mo<sub>2</sub>C and W<sub>2</sub>C, respectively, compared with the reported values of their commercial samples (Gao et al., 2014; Hussain et al., 2019a). In addition, the pore diameter vs. pore volume profile (Figure S6B) shows the mesoporous nature of chemically reduced Mo<sub>2</sub>C and W<sub>2</sub>C, with pore diameters of 14.9 and 21.4 nm and pore volumes of 0.003 and 0.009 cm<sup>3</sup>·g<sup>-1</sup>, respectively.

The HER electrocatalytic activities of Mo<sub>2</sub>C- and W<sub>2</sub>C-coated nickel foam (NF) electrodes were analyzed by linear sweep voltammogram (LSV) in 1 M KOH and 0.5 M H<sub>2</sub>SO<sub>4</sub> electrolyte

solutions (scan rate of 10 mV s<sup>-1</sup>, three-electrode setup). For the evaluation, a commercial Pt/C was used as an electrode, and the results were as follows. Figure 6A shows the LSV curves of commercial Pt/C and reduced Mo<sub>2</sub>C and W<sub>2</sub>C catalysts in a 0.5 M H<sub>2</sub>SO<sub>4</sub> solution. As anticipated, the commercial Pt/C catalyst showed the highest HER activity, which had an overpotential of ~-49 mV. For bare NF, Mo<sub>2</sub>C, and W<sub>2</sub>C, overpotentials of -423, -134, and -170 mV were needed to achieve 10 mAcm<sup>-2</sup> in acidic electrolyte, respectively, lower than those of the commercial samples (Vrubel and Hu, 2012; Chen et al., 2013). The overpotentials of the chemically reduced Mo<sub>2</sub>C and W<sub>2</sub>C were much closer to the recently reported values for carbide-based materials in acid medium, such as Mo<sub>2</sub>C encapsulated by nitrogen and phosphorus codoped carbon shells ( $\eta_{10\text{mA}/\text{cm}^2}$ @-260 mV) (Li et al., 2016), Mo<sub>2</sub>C nanoparticles embedded in chain-like Ketjenblack carbon ( $\eta_{10\text{mA}/\text{cm}^2}$ @-221 ~-263 mV) (Wang et al., 2017), porous MoC<sub>x</sub> nano octahedrons ( $\eta_{10\text{mA}/\text{cm}^2}$ @-142 mV) (Wu

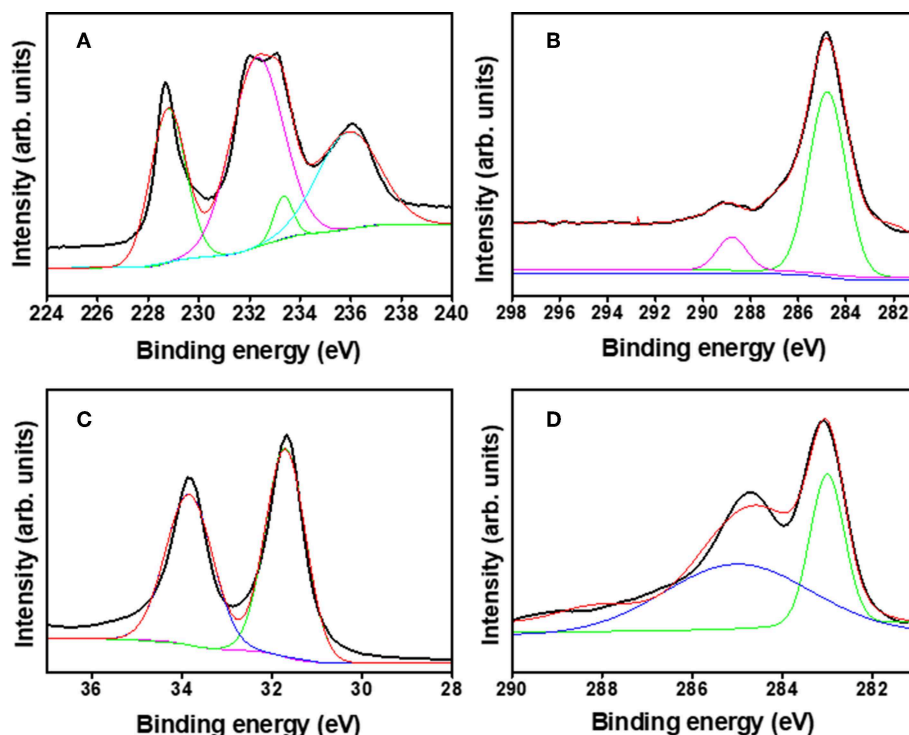


**FIGURE 5** | X-ray photoemission spectra: **(A)** Mo 3d, **(B)** C 1s binding energy spectra of Mo<sub>2</sub>C nanoparticles, **(C)** W 4f, and **(D)** C 1s binding energy spectra of W<sub>2</sub>C nanoparticles.

et al., 2015), 3D porous scaffold-like Mo<sub>2</sub>C/C nanosheet hybrids ( $\eta_{10\text{mA}/\text{cm}^2}@-233\text{ mV}$ ) (Wang et al., 2018), reduced graphene oxide-based Mo<sub>2</sub>C composites ( $\eta_{10\text{mA}/\text{cm}^2}@-206\text{ mV}$ ) (Ojha et al., 2016), Mo<sub>2</sub>C nanoparticle-decorated graphitic carbon sheets ( $\eta_{10\text{mA}/\text{cm}^2}@-200\sim 210\text{ mV}$ ) (Cui et al., 2014), Mo<sub>2</sub>C particles embedded in a sulfur and nitrogen codoped mesoporous carbon matrix ( $\eta_{10\text{mA}/\text{cm}^2}@-146\text{ mV}$ ) (An et al., 2017), and Mo<sub>2</sub>C NCs on vertically aligned graphene ( $\eta_{10\text{mA}/\text{cm}^2}@-152\text{ mV}$ ) (Fan et al., 2017). The electrocatalytic properties of Pt/C, Mo<sub>2</sub>C, and W<sub>2</sub>C catalysts were appraised in a 1 M KOH medium (**Figure 6B**). Similarly, the Pt/C, Mo<sub>2</sub>C, and W<sub>2</sub>C electrocatalysts produced  $-48$ ,  $-116$ , and  $-130\text{ mV}$  overpotentials to drive the  $10\text{ mAcm}^{-2}$  reaction in an alkaline electrolyte. The bare NF did not produce viable HER properties in a 1 M KOH medium. The observed results constitute a considerable advance over earlier results.

The Tafel slope signifies the characteristic activity acquired of an electrocatalyst and is derived using the Tafel equation for the HER. As shown in **Figures 6C,D**, Pt/C offers Tafel slopes of 43 and 48  $\text{mV.dec}^{-1}$  for acidic and alkaline electrolytes, respectively, which is comparable with the reported results (Fan et al., 2018). The extracted slope values from the Tafel plots were 83 and 86  $\text{mV.dec}^{-1}$  for the acidic and 65 and 100  $\text{mV.dec}^{-1}$  for the alkali for reduced Mo<sub>2</sub>C and W<sub>2</sub>C, respectively. These values indicate that the Volmer-Heyrovsky reaction step is obeyed for the whole HER process (Bockris and Potter, 1952; Yuan et al., 2018). Another

important parameter, the exchange current density ( $j_0$ ), was extracted to evaluate HER activity by extrapolating the linear region of the Tafel plot. A chemically reduced Mo<sub>2</sub>C catalyst displays  $j_0$  values of 0.846 and 0.131  $\text{mA cm}^{-2}$  in alkali and acidic media, respectively, while a chemically reduced W<sub>2</sub>C catalyst shows  $j_0$  values of 0.438 and 0.194  $\text{mA cm}^{-2}$ . The observed parameters are provided in **Table 1**. A detailed comparison of chemically reduced Mo<sub>2</sub>C and W<sub>2</sub>C HER parameters, with the reported carbide-based materials in alkaline and acidic media, are provided in **Tables S1, S2**, respectively.

The observed HER properties are credited to the reduced sizes of Mo<sub>2</sub>C and W<sub>2</sub>C nanostructures and their improved morphological properties in terms of edge sites.

High electrical conductivity allows for rapid ion/electron transfer between the active electrocatalyst edge sites and also provides a high interaction area between the electrolyte and the electrode, which in turn enhances the electrochemical performance. The charge transport mechanism was clarified by employing electrochemical impedance spectroscopy (EIS) studies to understand the HER mechanism of Mo<sub>2</sub>C and W<sub>2</sub>C nanoparticles at the interface between electrodes and electrolytes. The charge transfer properties with resistance ( $R_{\text{ct}}$ ) are exhibited for Pt/C in acidic and alkaline media as shown in **Figures S7A,B**. The lower  $R_{\text{ct}}$  values for chemically reduced Mo<sub>2</sub>C and W<sub>2</sub>C in acidic and alkaline media confirmed that they favor rapid electron transport in H<sub>2</sub> evolution (**Figures S7A,B**).

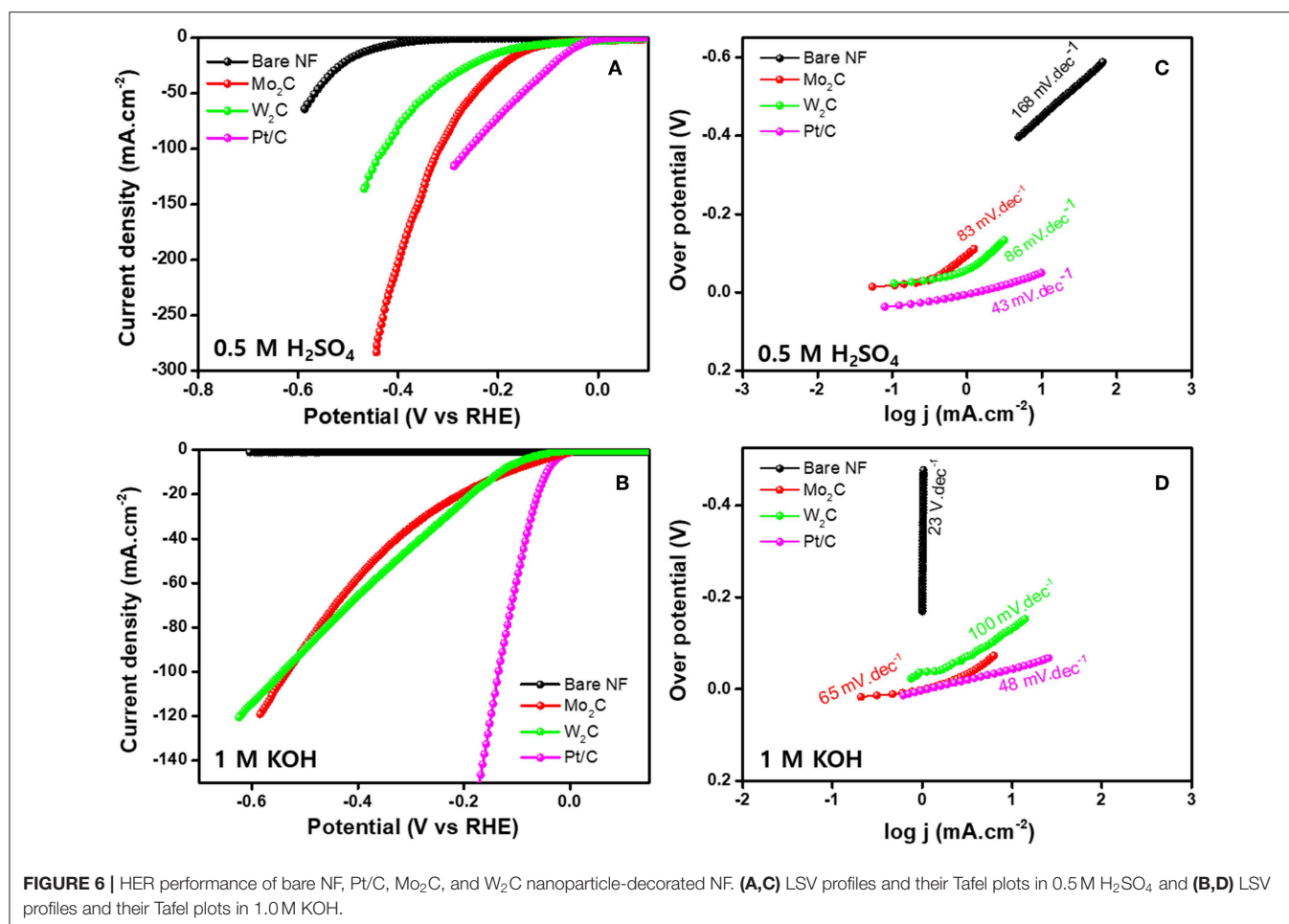


**FIGURE 6** | HER performance of bare NF, Pt/C, Mo<sub>2</sub>C, and W<sub>2</sub>C nanoparticle-decorated NF. **(A,C)** LSV profiles and their Tafel plots in 0.5 M H<sub>2</sub>SO<sub>4</sub> and **(B,D)** LSV profiles and their Tafel plots in 1.0 M KOH.

We estimated the electrochemically active surface area (ECSA) through cyclic voltammetry (CV), which was accomplished at different scan rates from 10 to 100 mVs<sup>-1</sup> in the non-Faradaic regions for Mo<sub>2</sub>C and W<sub>2</sub>C, as shown in **Figures S8A–D**, respectively (Zhou et al., 2016; Hussain et al., 2019a; Vikraman et al., 2019a). The double-layer capacitance ( $C_{dl}$ ) was extracted from the fitted slope value of the current differences ( $\Delta j_{a-c}$ ) of the cathodic and anodic peaks of CV profiles at 0.24 V vs. RHE (**Figure S8E**). The extracted  $C_{dl}$  values were 2.13 and 1.42 mF·cm<sup>-2</sup> in acid medium and 2.90 and 1.86 mF·cm<sup>-2</sup> in alkaline medium for Mo<sub>2</sub>C and W<sub>2</sub>C, respectively. The ECSA values were assessed through a previously described procedure (Vikraman et al., 2019a) and were 60.8 and 40.6 cm<sup>2</sup> in an acidic and 72.5 and 46.5 cm<sup>2</sup> in a alkaline medium for Mo<sub>2</sub>C and W<sub>2</sub>C, respectively, indicating higher HER activity for the Mo<sub>2</sub>C system. We estimated the amount of surface active sites using the method reported by Fei et al. (2015). The turnover frequency (TOF) values of Mo<sub>2</sub>C and W<sub>2</sub>C were calculated in the acidic and alkaline media. The TOF values of Mo<sub>2</sub>C are 0.005 and 0.037 H<sub>2</sub>·s<sup>-1</sup> at overpotentials of -134 and -116 mV, and those of W<sub>2</sub>C are 0.015 and 0.034 H<sub>2</sub>·s<sup>-1</sup> at overpotentials of -173 and -130 mV in acidic and alkaline media, respectively. The observed TOF values are comparable with

**TABLE 1** | Comparison of the electrochemical parameters of different electrocatalysts.

Electrolyte	Electrocatalysts	Tafel slope (mV·dec <sup>-1</sup> )	Overpotential (mV vs. RHE) @ 10 mA·cm <sup>-2</sup>	Exchange current density ( $j_0$ , mA·cm <sup>-2</sup> )
0.5 M H <sub>2</sub> SO <sub>4</sub>	Pt/C	43	-49	1.03
	Mo <sub>2</sub> C	83	-134	0.131
	W <sub>2</sub> C	86	-173	0.194
	Bare NF	168	-423	0.022
1 M KOH	Pt/C	48	-48	0.891
	Mo <sub>2</sub> C	65	-116	0.846
	W <sub>2</sub> C	100	-130	0.438
	Bare NF	-	-	-

previous reports (Chen et al., 2011; Fei et al., 2015; Ma L. et al., 2015; Zhang et al., 2017).

The robustness of the Mo<sub>2</sub>C and W<sub>2</sub>C catalysts was analyzed by carrying out chronoamperometric performances in 0.5 M H<sub>2</sub>SO<sub>4</sub> and in 1 M KOH for 20 h; the results are shown in

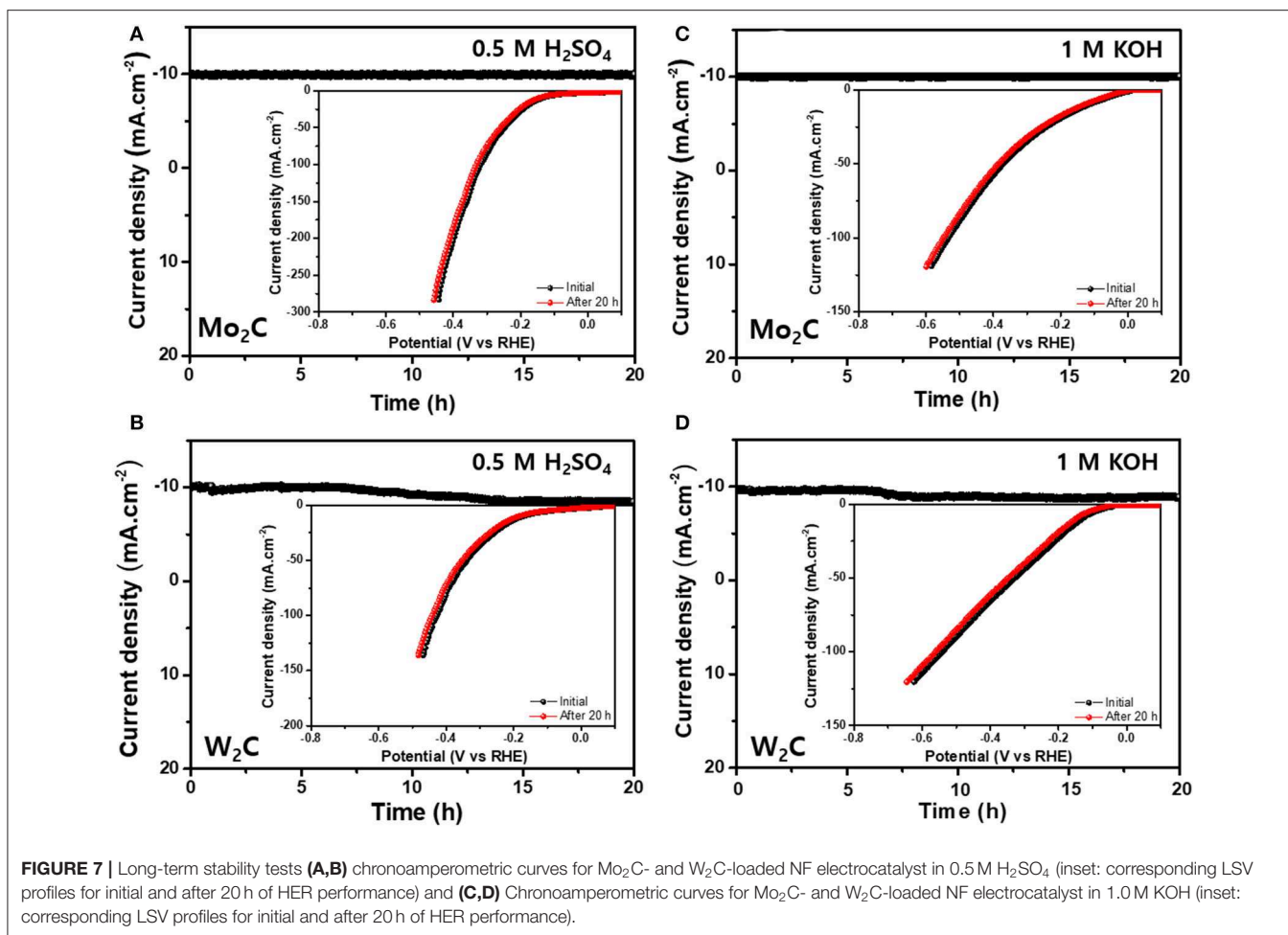


**FIGURE 7** | Long-term stability tests (A,B) chronoamperometric curves for Mo<sub>2</sub>C- and W<sub>2</sub>C-loaded NF electrocatalyst in 0.5 M H<sub>2</sub>SO<sub>4</sub> (inset: corresponding LSV profiles for initial and after 20 h of HER performance) and (C,D) Chronoamperometric curves for Mo<sub>2</sub>C- and W<sub>2</sub>C-loaded NF electrocatalyst in 1.0 M KOH (inset: corresponding LSV profiles for initial and after 20 h of HER performance).

**Figures 7A–D.** The LSV profiles of Mo<sub>2</sub>C and W<sub>2</sub>C catalysts were examined after 20 h of HER operation (−0.6 to 0.15 V vs. RHE at a scan rate of 10 mV s<sup>−1</sup>) in alkaline and acid media (Figure 7). The polarization curves revealed the robust nature of Mo<sub>2</sub>C after 20 h of working operation, whereas W<sub>2</sub>C showed slight degradation. Hence, the observed deliverables established the capability of chemically reduced Mo<sub>2</sub>C catalysts with long-term durability in alkaline and acidic media, which makes them interchangeable for high-cost materials.

Furthermore, the stability of the Mo<sub>2</sub>C and W<sub>2</sub>C catalysts was investigated by XPS and FESEM analysis after continuous 20 h-HER operation in electrolytic solution (acidic medium); the results are shown in Figures S9, S10. The observed results also confirm no dramatic changes in XPS and FESEM data after continuous 20 h HER operation.

## CONCLUSIONS

Chemically reduced Mo<sub>2</sub>C and W<sub>2</sub>C produced using an economical reduction method were successfully employed as electrocatalysts for application in HER. The observed HER results revealed that Mo<sub>2</sub>C and W<sub>2</sub>C nanoparticles had low overpotentials ( $\eta_{-10\text{mAcm}^{-2}} = -134$  and  $-116$  mV and  $-173$  and  $-130$  mV for Mo<sub>2</sub>C and W<sub>2</sub>C nanoparticles, respectively)

with small Tafel slopes (83 and 65 mV.dec<sup>−1</sup> and 86 and 100 mV.dec<sup>−1</sup> for Mo<sub>2</sub>C and W<sub>2</sub>C nanoparticles, respectively) in a 0.5 M H<sub>2</sub>SO<sub>4</sub> and in 1 M KOH electrolyte media. Both carbide catalysts showed strong stability in the alkaline and acidic media for over 20 h of operation. Thus, this work shows a viable way to synthesize nanostructured TMC-based electrocatalysts for hydrogen production.

## EXPERIMENTAL SECTION

### Materials and Methods

The commercial Mo<sub>2</sub>C and W<sub>2</sub>C chemicals of reagent grade were acquired from Sigma-Aldrich and were used without further purification. The following procedure was followed to prepare the chemically reduced Mo<sub>2</sub>C and W<sub>2</sub>C nanostructures (Hussain et al., 2019a). First, 2 g of commercial powder was well-disseminated in 100 mL of ethanol in a beaker to form a clear solution with the assistance of a room temperature stirring process. Subsequently, 50 mL of liquid ammonia solution was mixed with the black solution mixture, which was followed by a magnetic stirring at 85°C until the ethanol was completely evaporated from the mixture. The settled residue was then purified with de-ionized water and alcohol, sometimes using a centrifuge process, and the resultant material was placed in an

oven at 60°C for 6 h. Finally, the collected black powders were placed in a quartz tube, and their temperature was raised with a heating rate of 5°C/min to attain 850°C with the support of a CH<sub>4</sub>/Ar/H<sub>2</sub>-mixture gas flow (50 sccm). The final chemically reduced Mo<sub>2</sub>C and W<sub>2</sub>C samples were kept in a vacuum desiccator for further analysis.

## Electrochemical Measurements

The electrocatalytic HER properties were examined in an acid medium (0.5 M H<sub>2</sub>SO<sub>4</sub> solution) and an alkaline medium (1 M KOH) by using a typical three-electrode setup. A saturated calomel electrode (SCE) and a carbon rod were used as the reference and counter electrodes, respectively. For the preparation of a working electrode, a 10:80:10 weight ratio of poly(vinylidene fluoride), active materials (W<sub>2</sub>C and Mo<sub>2</sub>C), and carbon black was used with an N-methyl-2-pyrrolidone solvent. The resultant sample was coated onto NF and dried overnight at 90°C. Mo<sub>2</sub>C- and W<sub>2</sub>C-loaded NF was employed as the working electrode. The LSV was recorded using a scan rate of 10 mV s<sup>-1</sup> at room temperature. All the LSV performances were completed using SCE and then referenced to a reversible hydrogen electrode (RHE) scale using the following equation: E (RHE) = E (SCE) + E° (SCE) + 0.059 pH. An electrochemical impedance spectroscopy (EIS) study was performed within the 0.1 Hz to 1 MHz frequency with a perturbation voltage of 10 mV.

## Characterization

Mo<sub>2</sub>C and W<sub>2</sub>C nanoparticles were studied using Raman spectroscopy (Renishaw Invia RE04, Ar laser—512 nm), FE-SEM (HITACHI S-4700), a Rigaku Ultima IV diffractometer with Cu-Kα radiation (0.154 nm), JEOL-2010F TEM with the help of Gatan DM software (version 3.0), PHI 5000 Versa Probe XPS, and a 3Flex surface characterization analyzer for nitrogen adsorption and desorption measurement at 77 K (Micromeritics, USA).

## REFERENCES

- An, K., and Xu, X. (2019). Mo<sub>2</sub>C based electrocatalyst with nitrogen doped three-dimensional mesoporous carbon as matrix, synthesis and HER activity study. *Electrochim. Acta* 293, 348–355. doi: 10.1016/j.electacta.2018.10.050
- An, K., Xu, X., and Liu, X. (2017). Mo<sub>2</sub>C-based electrocatalyst with biomass-derived sulfur and nitrogen co-doped carbon as a matrix for hydrogen evolution and organic pollutant removal. *ACS Sustain. Chem. Eng.* 6, 1446–1455. doi: 10.1021/acssuschemeng.7b03882
- Ang, H., Wang, H., Li, B., Zong, Y., Wang, X., and Yan, Q. (2016). 3D hierarchical porous Mo<sub>2</sub>C for efficient hydrogen evolution. *Small* 12, 2859–2865. doi: 10.1002/smll.201600110
- Berglund, S. P., He, H., Chemelewski, W. D., Celio, H., Dolocan, A., and Mullins, C. B. (2014). p-Si/W<sub>2</sub>C and p-Si/W<sub>2</sub>C/Pt photocathodes for the hydrogen evolution reaction. *J. Am. Chem. Soc.* 136, 1535–1544. doi: 10.1021/ja411604k
- Bockris, J. M., and Potter, E. (1952). The mechanism of the cathodic hydrogen evolution reaction. *J. Electrochem. Soc.* 99, 169–186. doi: 10.1149/1.2779692
- Chen, W. F., Wang, C. H., Sasaki, K., Marinkovic, N., Xu, W., Muckerman, J., et al. (2013). Highly active and durable nanostructured molybdenum carbide electrocatalysts for hydrogen production. *Energy Environ. Sci.* 6, 943–951. doi: 10.1039/c2ee23891h
- Chen, Y. Y., Zhang, Y., Jiang, W. J., Zhang, X., Dai, Z., Wan, L. J., et al. (2016). Pomegranate-like N, P-doped Mo<sub>2</sub>C@C nanospheres as highly active

## DATA AVAILABILITY STATEMENT

All datasets generated for this study are included in the article/**Supplementary Material**.

## AUTHOR CONTRIBUTIONS

SH and JJ prepared the manuscript. SH performed the material synthesis. DV and AF actively took part in the characterization of catalysts. WS and K-SA performed XPS measurement and physical characterization of synthesized materials. H-SK, S-HC, and JJ did planning, design experimental work, and discussion. JJ edited the paper.

## FUNDING

This research was supported by the Basic Science Research Program through the National Research Foundation of Korea (NRF), funded by the Ministry of Education (2015M3A7B7045194, 2017R1C1B5076952, and 2016M3A7B4909942), by the MOTIE (10052928) and the KSRC (Korea Semiconductor Research Consortium) support programs for the development of future semiconductor devices. This work was supported by the Korea Institute of Energy Technology Evaluation and Planning (KETEP) and the Ministry of Trade, Industry & Energy (MOTIE) of the Republic of Korea (20172010106080).

## SUPPLEMENTARY MATERIAL

The Supplementary Material for this article can be found online at: <https://www.frontiersin.org/articles/10.3389/fchem.2019.00716/full#supplementary-material>

electrocatalysts for alkaline hydrogen evolution. *ACS Nano* 10, 8851–8860. doi: 10.1021/acsnano.6b04725

Chen, Z., Cummins, D., Reinecke, B. N., Clark, E., Sunkara, M. K., and Jaramillo, T. F. (2011). Core-shell MoO<sub>3</sub>-MoS<sub>2</sub> nanowires for hydrogen evolution: a functional design for electrocatalytic materials. *Nano Lett.* 11, 4168–4175. doi: 10.1021/nl2020476

Colton, R. J., Huang, J. T. J., and Rabalais, J. W. (1975). Electronic structure of tungsten carbide and its catalytic behavior. *Chem. Phys. Lett.* 34, 337–339. doi: 10.1016/0009-2614(75)85287-0

Cui, W., Cheng, N., Liu, Q., Ge, C., Asiri, A. M., and Sun, X. (2014). Mo<sub>2</sub>C nanoparticles decorated graphitic carbon sheets: biopolymer-derived solid-state synthesis and application as an efficient electrocatalyst for hydrogen generation. *ACS Catal.* 4, 2658–2661. doi: 10.1021/cs5005294

Fan, M., Zheng, Y., Li, A., Ma, Y., Huo, Q., Qiao, Z. A., et al. (2018). Sprout-like growth of mesoporous Mo<sub>2</sub>C/NC nanonetworks as efficient electrocatalysts for hydrogen evolution. *ChemCatChem* 10, 625–631. doi: 10.1002/cctc.201701417

Fan, X., Liu, Y., Peng, Z., Zhang, Z., Zhou, H., Zhang, X., et al. (2017). Atomic H-induced Mo<sub>2</sub>C hybrid as an active and stable bifunctional electrocatalyst. *ACS Nano* 11, 384–394. doi: 10.1021/acsnano.6b06089

Fei, H., Dong, J., Arellano-Jiménez, M. J., Ye, G., Dong Kim, N., Samuel, E. L. G., et al. (2015). Atomic cobalt on nitrogen-doped graphene for hydrogen generation. *Nat. Commun.* 6:8668. doi: 10.1038/ncomms9668

- Gao, Q., Zhao, X., Xiao, Y., Zhao, D., and Cao, M. (2014). A mild route to mesoporous Mo<sub>2</sub>C–C hybrid nanospheres for high performance lithium-ion batteries. *Nanoscale* 6, 6151–6157. doi: 10.1039/c3nr06678a
- Gong, Q., Wang, Y., Hu, Q., Zhou, J., Feng, R., Duchesne, P. N., et al. (2016). Ultrasmall and phase-pure W<sub>2</sub>C nanoparticles for efficient electrocatalytic and photoelectrochemical hydrogen evolution. *Nat. Commun.* 7:13216. doi: 10.1038/ncomms13216
- Huang, Y., Gong, Q., Song, X., Feng, K., Nie, K., Zhao, F., et al. (2016). Mo<sub>2</sub>C nanoparticles dispersed on hierarchical carbon microflowers for efficient electrocatalytic hydrogen evolution. *ACS Nano* 10, 11337–11343. doi: 10.1021/acsnano.6b06580
- Hussain, S., Akbar, K., Vikraman, D., Afzal, R. A., Song, W., An, K. S., et al. (2018). WS<sub>(1-x)</sub>Se<sub>x</sub> nanoparticles decorated three-dimensional graphene on nickel foam: a robust and highly efficient electrocatalyst for the hydrogen evolution reaction. *Nanomaterials* 8:929. doi: 10.3390/nano8110929
- Hussain, S., Vikraman, D., Akbar, K., Naqvi, B. A., Abbas, S. M., Kim, H. S., et al. (2019a). Fabrication of MoSe<sub>2</sub> decorated three-dimensional graphene composites structure as a highly stable electrocatalyst for improved hydrogen evolution reaction. *Renew. Energy* 143, 1659–1669. doi: 10.1016/j.renene.2019.05.126
- Hussain, S., Zaidi, S. A., Vikraman, D., Kim, H. S., Jung, J. (2019b). Facile preparation of molybdenum carbide (Mo<sub>2</sub>C) nanoparticles and its effective utilization in electrochemical sensing of folic acid via imprinting. *Biosens. Bioelectron.* 140:111330. doi: 10.1016/j.bios.2019.111330
- Ishii, T., Yamada, K., Osuga, N., Imashiro, Y., and Ozaki, J. I. (2016). Single-step synthesis of W<sub>2</sub>C nanoparticle-dispersed carbon electrocatalysts for hydrogen evolution reactions utilizing phosphate groups on carbon edge sites. *ACS Omega* 1, 689–695. doi: 10.1021/acsomega.6b00179
- Jacobsson, T. J., Fjällström, V., Sahlberg, M., Edoff, M., and Edvinsson, T. (2013). A monolithic device for solar water splitting based on series interconnected thin film absorbers reaching over 10% solar-to-hydrogen efficiency. *Energy Environ. Sci.* 6, 3676–3683. doi: 10.1039/c3ee42519c
- Ko, Y. J., Cho, J. M., Kim, I., Jeong, D. S., Lee, K. S., Park, J. K., et al. (2017). Tungsten carbide nanowalls as electrocatalyst for hydrogen evolution reaction: new approach to durability issue. *Appl. Catal. B Environ.* 203, 684–691. doi: 10.1016/j.apcatb.2016.10.085
- Kou, Z., Wang, T., Cai, Y., Guan, C., Pu, Z., Zhu, C., et al. (2018). Ultrafine molybdenum carbide nanocrystals confined in carbon foams via a colloid-confinement route for efficient hydrogen production. *Small Methods* 2:1700396. doi: 10.1002/smt.201700396
- Kou, Z., Wang, T., Pu, Z., Wu, L., Xi, K., and Mu, S. (2019). Realizing the extraction of carbon from WC for in situ formation of W/WC heterostructures with efficient photoelectrochemical hydrogen evolution. *Nanoscale Horizons* 4, 196–201. doi: 10.1039/C8NH00275D
- Kou, Z., Xi, K., Pu, Z., and Mu, S. (2017). Constructing carbon-cohered high-index (222) faceted tantalum carbide nanocrystals as a robust hydrogen evolution catalyst. *Nano Energy* 36, 374–380. doi: 10.1016/j.nanoen.2017.04.057
- Laursen, A. B., Kegnæs, S., Dahl, S., and Chorkendorff, I. (2012). Molybdenum sulfides—efficient and viable materials for electro- and photoelectrocatalytic hydrogen evolution. *Energy Environ. Sci.* 5, 5577–5591. doi: 10.1039/c2ee02618j
- Li, J. S., Wang, Y., Liu, C. H., Li, S. L., Wang, Y. G., Dong, L. Z., et al. (2016). Coupled molybdenum carbide and reduced graphene oxide electrocatalysts for efficient hydrogen evolution. *Nat. Commun.* 7:11204. doi: 10.1038/ncomms11204
- Liang, Q., Jin, H., Wang, Z., Xiong, Y., Yuan, S., Zeng, X., et al. (2019). Metal-organic frameworks derived reverse-encapsulation Co-NC@ Mo<sub>2</sub>C complex for efficient overall water splitting. *Nano Energy* 57, 746–752. doi: 10.1016/j.nanoen.2018.12.060
- Lin, Z., Cai, L., Lu, W., and Chai, Y. (2017). Phase and facet control of molybdenum carbide nanosheet observed by *in situ* TEM. *Small* 13:1700051. doi: 10.1002/smll.201700051
- Lv, C., Huang, Z., Yang, Q., Wei, G., Chen, Z., Humphrey, M. G., et al. (2017). Ultrafast synthesis of molybdenum carbide nanoparticles for efficient hydrogen generation. *J. Mater. Chem. A* 5, 22805–22812. doi: 10.1039/C7TA06266D
- Lv, Y., and Wang, X. (2017). Nonprecious metal phosphides as catalysts for hydrogen evolution, oxygen reduction and evolution reactions. *Catal. Sci. Technol.* 7, 3676–3691. doi: 10.1039/C7CY00715A
- Ma, F. X., Wu, H. B., Xia, B. Y., Xu, C. Y., and Lou, X. W. (2015). Hierarchical β-Mo<sub>2</sub>C nanotubes organized by ultrathin nanosheets as a highly efficient electrocatalyst for hydrogen production. *Angew. Chem. Int. Ed.* 54, 15395–15399. doi: 10.1002/anie.201508715
- Ma, L., Ting, L. R. L., Molinari, V., Giordano, C., and Yeo, B. S. (2015). Efficient hydrogen evolution reaction catalyzed by molybdenum carbide and molybdenum nitride nanocatalysts synthesized via the urea glass route. *J. Mater. Chem. A* 3, 8361–8368. doi: 10.1039/C5TA00139K
- Ma, R., Zhou, Y., Chen, Y., Li, P., Liu, Q., and Wang, J. (2015). Ultrafine molybdenum carbide nanoparticles composited with carbon as a highly active hydrogen-evolution electrocatalyst. *Angew. Chem.* 127, 14936–14940. doi: 10.1002/ange.201506727
- Neylon, M., Choi, S., Kwon, H., Curry, K., and Thompson, L. (1999). Catalytic properties of early transition metal nitrides and carbides: n-butane hydrogenolysis, dehydrogenation and isomerization. *Appl. Catal. A Gen.* 183, 253–263. doi: 10.1016/S0926-860X(99)00053-8
- Ojha, K., Saha, S., Kolev, H., Kumar, B., and Ganguli, A. K. (2016). Composites of graphene-Mo<sub>2</sub>C rods: highly active and stable electrocatalyst for hydrogen evolution reaction. *Electrochim. Acta* 193, 268–274. doi: 10.1016/j.electacta.2016.02.081
- Pan, L. F., Li, Y. H., Yang, S., Liu, P. F., Yu, M. Q., and Yang, H. G. (2014). Molybdenum carbide stabilized on graphene with high electrocatalytic activity for hydrogen evolution reaction. *Chem. Commun.* 50, 13135–13137. doi: 10.1039/C4CC05698A
- Pei, Y., Cheng, Y., Chen, J., Smith, W., Dong, P., Ajayan, P. M., et al. (2018). Recent developments of transition metal phosphides as catalysts in the energy conversion field. *J. Mater. Chem. A* 6, 23220–23243. doi: 10.1039/C8TA09454C
- Peng, L., Nie, Y., Zhang, L., Xiang, R., Wang, J., Chen, H., et al. (2017). Self-assembly and reshaping-assisted synthesis of molybdenum carbide supported on ultrathin nitrogen-doped graphitic carbon lamellas for the hydrogen evolution reaction. *ChemCatChem* 9, 1588–1593. doi: 10.1002/cctc.201700239
- Peng, S., Li, L., Han, X., Sun, W., Srinivasan, M., Mhaisalkar, S. G., et al. (2014). Cobalt sulfide nanosheet/graphene/carbon nanotube nanocomposites as flexible electrodes for hydrogen evolution. *Angew. Chem.* 126, 12802–12807. doi: 10.1002/ange.201408876
- Pu, Z., Wang, M., Kou, Z., Amiin, I. S., and Mu, S. (2016). Mo<sub>2</sub>C quantum dot embedded chitosan-derived nitrogen-doped carbon for efficient hydrogen evolution in a broad pH range. *Chem. Commun.* 52, 12753–12756. doi: 10.1039/C6CC06267A
- Ren, X., Wei, Q., Ren, P., Wang, Y., and Chen, R. (2018). Synthesis of flower-like MoSe<sub>2</sub>@MoS<sub>2</sub> nanocomposites as the high efficient water splitting electrocatalyst. *Mater. Lett.* 231, 213–216. doi: 10.1016/j.matlet.2018.08.049
- Seok, J., Lee, J. H., Cho, S., Ji, B., Kim, H. W., Kwon, M., et al. (2017). Active hydrogen evolution through lattice distortion in metallic MoTe<sub>2</sub>, 2D. *Materials* 4:025061. doi: 10.1088/2053-1583/aa659d
- Shi, Z., Nie, K., Shao, Z. J., Gao, B., Lin, H., Zhang, H., et al. (2017). Phosphorus-Mo<sub>2</sub>C@carbon nanowires toward efficient electrochemical hydrogen evolution: composition, structural and electronic regulation. *Energy Environ. Sci.* 10, 1262–1271. doi: 10.1039/C7EE00388A
- Tang, C., Sun, A., Xu, Y., Wu, Z., and Wang, D. (2015). High specific surface area Mo<sub>2</sub>C nanoparticles as an efficient electrocatalyst for hydrogen evolution. *J. Power Sour.* 296, 18–22. doi: 10.1016/j.jpowsour.2015.07.016
- Vikraman, D., Akbar, K., Hussain, S., Yoo, G., Jang, J. Y., Chun, S. H., et al. (2017). Direct synthesis of thickness-tunable MoS<sub>2</sub> quantum dot thin layers: optical, structural and electrical properties and their application to hydrogen evolution. *Nano Energy* 35, 101–114. doi: 10.1016/j.nanoen.2017.03.031
- Vikraman, D., Hussain, S., Akbar, K., Karuppasamy, K., Chun, S. H., Jung, J., et al. (2019a). Design of basal plane edges in metal-doped nanostripes-structured MoSe<sub>2</sub> atomic layers to enhance hydrogen evolution reaction activity. *ACS Sustain. Chem. Eng.* 7, 458–469. doi: 10.1021/acssuschemeng.8b03921
- Vikraman, D., Hussain, S., Akbar, K., Truong, L., Kathalingam, A., S.-, Chun, H., et al. (2018). Improved hydrogen evolution reaction performance using MoS<sub>2</sub>-WS<sub>2</sub> heterostructures by physicochemical process. *ACS Sustain. Chem. Eng.* 6, 8400–8409. doi: 10.1021/acssuschemeng.8b00524
- Vikraman, D., Hussain, S., Truong, L., Karuppasamy, K., Kim, H. J., Maiyalagan, T., et al. (2019b). Fabrication of MoS<sub>2</sub>/WS<sub>2</sub> heterostructures as electrocatalyst for enhanced hydrogen evolution reaction. *Appl. Surf. Sci.* 480, 611–620. doi: 10.1016/j.apsusc.2019.02.236

- Vrubel, H., and Hu, X. (2012). Molybdenum boride and carbide catalyze hydrogen evolution in both acidic and basic solutions. *Angew. Chem.* 124, 12875–12878. doi: 10.1002/ange.201207111
- Wan, C., Regmi, Y. N., and Leonard, B. M. (2014). Multiple phases of molybdenum carbide as electrocatalysts for the hydrogen evolution reaction. *Angew. Chem.* 126, 6525–6528. doi: 10.1002/ange.201402998
- Wang, D., Guo, T., and Wu, Z. (2018). Hierarchical Mo<sub>2</sub>C/C scaffolds organized by nanosheets as highly efficient electrocatalysts for hydrogen production. *ACS Sustain. Chem. Eng.* 6, 13995–14003. doi: 10.1021/acssuschemeng.8b02469
- Wang, D., Wang, J., Luo, X., Wu, Z., and Ye, L. (2017). *In situ* preparation of Mo<sub>2</sub>C nanoparticles embedded in ketjenblack carbon as highly efficient electrocatalysts for hydrogen evolution. *ACS Sustain. Chem. Eng.* 6, 983–990. doi: 10.1021/acssuschemeng.7b03317
- Wu, H. B., Xia, B. Y., Yu, L., Yu, X. Y., and Lou, X. W. D. (2015). Porous molybdenum carbide nano-octahedrons synthesized via confined carburization in metal-organic frameworks for efficient hydrogen production. *Nat. Commun.* 6:6512. doi: 10.1038/ncomms7512
- Wu, Z. Y., Hu, B. C., Wu, P., Liang, H. W., Yu, Z. L., Lin, Y., et al. (2016). Mo<sub>2</sub>C nanoparticles embedded within bacterial cellulose-derived 3D N-doped carbon nanofiber networks for efficient hydrogen evolution. *NPG Asia Mater.* 8:e288. doi: 10.1038/am.2016.87
- Yan, G., Wu, C., Tan, H., Feng, X., Yan, L., Zang, H., et al. (2017). N-Carbon coated P-W<sub>2</sub>C composite as efficient electrocatalyst for hydrogen evolution reactions over the whole pH range. *J. Mater. Chem. A* 5, 765–772. doi: 10.1039/C6TA09052D
- Youn, D. H., Han, S., Kim, J. Y., Kim, J. Y., Park, H., Choi, S. H., et al. (2014). Highly active and stable hydrogen evolution electrocatalysts based on molybdenum compounds on carbon nanotube–graphene hybrid support. *ACS Nano* 8, 5164–5173. doi: 10.1021/nn5012144
- Yu, F., Gao, Y., Lang, Z., Ma, Y., Yin, L., Du, J., et al. (2018). Electrocatalytic performance of ultrasmall Mo 2C affected by different transition metal dopants in hydrogen evolution reaction. *Nanoscale* 10, 6080–6087. doi: 10.1039/C8NR00908B
- Yuan, W., Huang, Q., Yang, X., Cui, Z., Zhu, S., Li, Z., et al. (2018). Two-dimensional lamellar Mo<sub>2</sub>C for electrochemical hydrogen production: insights into the origin of HER activity in acid and alkaline electrolytes. *ACS Appl. Mater. Interfaces* 10, 40500–40508. doi: 10.1021/acsami.8b13215
- Zhang, L. N., Ma, Y. Y., Lang, Z. L., Wang, Y. H., Khan, S. U., Yan, G., et al. (2018). Ultrafine cable-like WC/W 2 C heterojunction nanowires covered by graphitic carbon towards highly efficient electrocatalytic hydrogen evolution. *J. Mater. Chem. A* 6, 15395–15403. doi: 10.1039/C8TA05007D
- Zhang, R., Wang, X., Yu, S., Wen, T., Zhu, X., Yang, F., et al. (2017). Ternary NiCo<sub>2</sub>Px nanowires as pH-universal electrocatalysts for highly efficient hydrogen evolution reaction. *Adv. Mater.* 29:1605502. doi: 10.1002/adma.201605502
- Zhou, H., Yu, F., Huang, Y., Sun, J., Zhu, Z., Nielsen, R. J., et al. (2016). Efficient hydrogen evolution by ternary molybdenum sulfoselenide particles on self-standing porous nickel diselenide foam. *Nat. Commun.* 7:12765. doi: 10.1038/ncomms12765
- Zhu, J., Lu, X., and Wang, L. (2016). Synthesis of a MoO<sub>3</sub>/Ti<sub>3</sub>C<sub>2</sub>T<sub>x</sub> composite with enhanced capacitive performance for supercapacitors. *RSC Adv.* 6, 98506–98513. doi: 10.1039/C6RA15651G

**Conflict of Interest:** The authors declare that the research was conducted in the absence of any commercial or financial relationships that could be construed as a potential conflict of interest.

Copyright © 2019 Hussain, Vikraman, Feroze, Song, An, Kim, Chun and Jung. This is an open-access article distributed under the terms of the Creative Commons Attribution License (CC BY). The use, distribution or reproduction in other forums is permitted, provided the original author(s) and the copyright owner(s) are credited and that the original publication in this journal is cited, in accordance with accepted academic practice. No use, distribution or reproduction is permitted which does not comply with these terms.